Gaussian and sech approximations of mode field profiles in photonic crystal fibers

doi: 10.1109/LPT.2004.824950

Gaussian and Sech Approximations of Mode Field Profiles in Photonic Crystal Fibers

Toshihiko Hirooka, *Member, IEEE*, Yusuke Hori, and Masataka Nakazawa, *Fellow, IEEE*

***Abstract*—We propose using the least square method for approximating the electrical field distribution of the fundamental mode in photonic crystal fibers (PCFs) by using a Gaussian and a hyperbolic-secant (sech) function. It is shown that the mode field can be fitted closely to a Gaussian for large d/Λ values (i.e., for strongly guiding structures). For small d/Λ values (for weakly guiding structures), a sech function fits the mode field well because the field gradually extends into the cladding region, implying that the analogy of PCFs with step index fibers is not applicable in this regime.**

***Index Terms*—Least square approximation, mode field diameter (MFD), photonic crystal fiber (PCF), spot size.**

I. Introduction

PHOTONIC crystal fibers (PCFs), which have a silica core and air holes in their cladding, guide light by total internal reflection caused by the effective index difference between the core and the cladding [1]. In such PCFs, the effective refractive index of the cladding $n_{\rm clad}$ can be varied by changing the hole pitch Λ and the hole diameter d. This offers a number of unique properties that cannot be achieved in standard step-index fibers (SIFs). For example, the effective V value (normalized frequency) $V_{\rm eff}$ is saturated against Λ/λ, where λ is the wavelength, resulting in single-mode operation over an ultrawide bandwidth [2]. A small change in Λ and d also enables flexible control of the waveguide dispersion and the effective mode area, which yields attractive features such as ultraflattened dispersion [3], zero dispersion at visible wavelengths [4], and low or high nonlinearity [5], [6].

A fundamental parameter that characterizes the mode field profile of fibers is the mode field diameter (MFD). The MFD indicates how widely the mode field is distributed in the radial direction against the core diameter, which is an important factor in estimating the splice loss, the source-to-fiber coupling efficiency, and reflection. For a simple evaluation of the MFD, the mode field profile is approximated by a specific function. In SIFs, it is well known that the field distribution of the fundamental mode is approximated by a Gaussian with high accuracy [7]. In PCFs, however, it is reported that an analytical expression based on the analogy with SIFs may not always be valid [8]–[11].

In this letter, we propose a simple method for approximating the electrical field distribution of the $\rm HE_{11}$ mode in PCFs that uses Gaussian and hyperbolic-secant (sech) functions. The least square approximation method was used to obtain the analytic expressions. In PCFs with a large air-filling fraction in the cladding, the mode field is still found to be a Gaussian. However, in PCFs with a small air-filling fraction, such as those used for achieving ultraflattened dispersion [3] and large mode area [5], the tail of the mode field extends well into the cladding. In this regime, the field distribution is much closer to a sech function, which decays more slowly in the tail than a Gaussian.

Manuscript received November 7, 2003; revised December 5, 2003.

The authors are with the Research Institute of Electrical Communication, Tohoku University, Sendai 980-8577, Japan (e-mail: hirooka@riec.tohoku.ac.jp).

Digital Object Identifier 10.1109/LPT.2004.824950

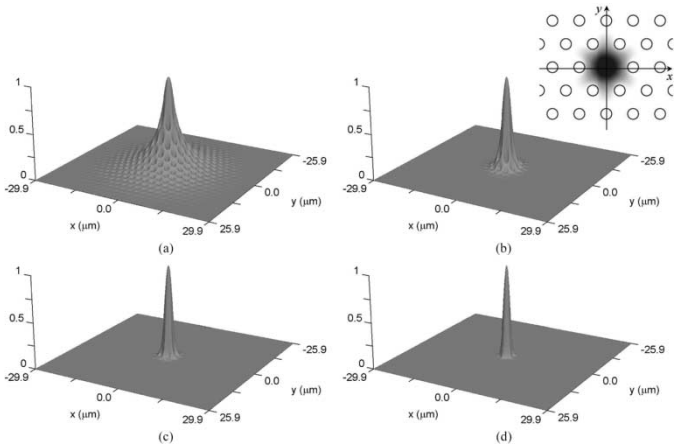

Fig. 1. Field distribution of the fundamental mode of PCF with (a) $d = 0.46$ μm ($d/\Lambda = 0.2$), (b) 0.92 μm ($d/\Lambda = 0.4$), (c) 1.38 μm ($d/\Lambda = 0.6$), and (d) 1.84 μm ($d/\Lambda = 0.8$). The inset shows the air hole structure of the PCF and the mode field distribution when $d/\Lambda = 0.4$.

II. Analysis

We used the semivector beam propagation method to compute the field profile of the $\rm HE_{11}$ mode of PCF [12]. Fig. 1 shows the mode field profile for the wavelength $\lambda = 1.55$ μm, the hole pitch $\Lambda = 2.3$ μm, and the hole diameters [Fig. 1(a)] $d = 0.46$ μm ($d/\Lambda = 0.2$), [Fig. 1(b)] 0.92 μm ($d/\Lambda = 0.4$), [Fig. 1(c)] 1.38 μm ($d/\Lambda = 0.6$), and [Fig. 1(d)] 1.84 μm ($d/\Lambda = 0.8$). It should be noted that, in this figure, the field is strongly confined in the core when d is large, whereas, for a small d, the tail of the confined field extends further into the cladding and decays slowly. The inset of Fig. 1 shows the air-hole geometry of the PCF and the field distribution when $d/\Lambda = 0.4$, in which the field extends into the cladding avoiding the air holes. In this regime, the mode field is expected to be closer to a sech function than a Gaussian.

Here, the least square approximation is used to fit the actual PCF mode field to Gaussian and sech functions, and analyze which function provides better fitting of the mode field distribution for different d/Λ values. Let us assume that a PCF mode field $\phi(x, y)$ is approximated by a Gaussian

$$\phi_G(x, y) = A \exp\left(-\frac{x^2 + y^2}{w^2}\right) \tag{1}$$

where $A = (1/w)\sqrt{2/\pi}$ so that the optical power is normalized to one. The least square approximation of $\phi(x, y)$ by $\phi_G(x, y)$ is obtained when the least square error

$$I(w) = \int_{-\infty}^{\infty}\int_{-\infty}^{\infty} [\phi(x,y) - \phi_G(x,y)]^2\, dxdy$$
$$= 2 - \frac{2}{w}\sqrt{\frac{2}{\pi}}\int_{-\infty}^{\infty}\int_{-\infty}^{\infty} \phi(x,y)\exp\left(-\frac{x^2+y^2}{w^2}\right)dxdy \tag{2}$$

is minimized with respect to w. From the condition $dI/dw = 0$, we find the following:

$$w = \left[\frac{2\int\int_{-\infty}^{\infty}(x^2+y^2)\phi(x,y)\exp\left(-\frac{x^2+y^2}{w^2}\right)dxdy}{\int\int_{-\infty}^{\infty}\phi(x,y)\exp\left(-\frac{x^2+y^2}{w^2}\right)dxdy}\right]^{\frac{1}{2}} \tag{3}$$

in which the parameter w minimizes $I(w)$. Since (3) contains w on both sides, we solve this equation iteratively starting from a proper initial value w_0. Note that the $w(2w)$ thus obtained corresponds to the spot size (MFD) of the mode field $\phi(x, y)$. By substituting w into (1), we finally obtain the Gaussian approximation $\phi_G(x, y)$.

Approximation by a sech function can be similarly formulated. When $\phi(x, y)$ is fitted to a sech function

$$\phi_S(x,y) = A\,\mathrm{sech}\left(\frac{x}{w}\right)\mathrm{sech}\left(\frac{y}{w}\right) \tag{4}$$

by the least square approximation, where $A = 1/2w$, the least square error involved with the approximation

$$I(w) = \int_{-\infty}^{\infty}\int_{-\infty}^{\infty} [\phi(x,y) - \phi_S(x,y)]^2\, dxdy$$
$$= 2 - \frac{1}{w}\int_{-\infty}^{\infty}\int_{-\infty}^{\infty} \phi(x,y)\mathrm{sech}\left(\frac{x}{w}\right)\mathrm{sech}\left(\frac{y}{w}\right)dxdy \tag{5}$$

must be minimized with respect to w. The value of w that minimizes $I(w)$ is obtained as a solution of (6), shown at bottom of page. As with (3), (6) is solved iteratively.

III. Numerical Results

We carried out a least square approximation for mode field distributions of PCFs with $d/\Lambda = 0.8$ and 0.4, shown in Fig. 1(d) and (b), respectively. In this case, the mode field of PCF with $d/\Lambda = 0.8$ is approximated by a Gaussian $\phi_G(x, y)$ by using (3). The result is shown by thick and thin solid curves in Fig. 2, corresponding to $\phi(x, y)$ and $\phi_G(x, y)$, respectively.

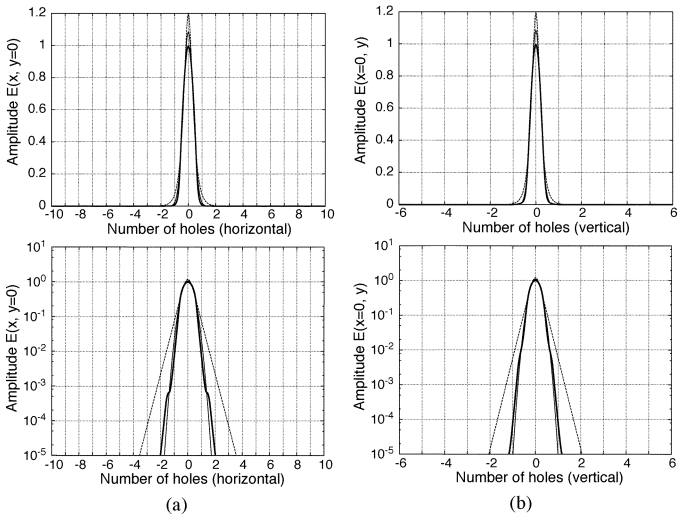

Fig. 2. Comparison of the actual PCF field distribution (thick solid curve) with the fitted Gaussian (thin solid curve) and sech (dotted curve) profile for $d/\Lambda = 0.8$. Linear (above) and log (below) scales. The mode is plotted along (a) x and (b) y axis.

In this figure, we plot the mode field on linear and log scales along [Fig. 2(a)] the x axis ($y = 0$) and [Fig. 2(b)] the y axis ($x = 0$) of the inset of Fig. 1, respectively. The grid lines plotted along the horizontal axis in Fig. 2(a) and (b) denote the location of the air hole centers on the x and y axes, respectively. These results show that the mode field is confined strongly in the core and, hence, the Gaussian approximation is accurate. Indeed, fitting the mode field to the sech function $\phi_S(x, y)$, shown as dotted curves, does not describe the mode profile correctly.

Fig. 3 shows the result when $d/\Lambda = 0.4$. We note in this figure that the tail of the mode field $\phi(x, y)$ (thick solid curves) distributed in the cladding fits less closely to a Gaussian profile $\phi_G(x, y)$ (thin solid curves). The mode field is then approximated by a sech profile $\phi_S(x, y)$ by using (6). The result is shown as dotted curves in Fig. 3, in which a tail of the mode field is now found to fit well with a sech function. It should be noted that, because of the mode field dips, which may be called "modulation," caused by the presence of the air holes, only the envelope of the mode field is fitted by a sech function. This approximation is valid for small d/Λ values.

Fig. 4 shows the mode field profile when the wavelength is 1.0 μm, for $d/\Lambda = 0.8$ [Fig. 4(a)] and 0.4 [Fig. 4(b)]. Fig. 4(a) and (b) fit well to a Gaussian and sech function, respectively. By comparing these results with the results for $\lambda = 1.55$ μm (namely, comparing Fig. 2(a) and Fig. 4(a) for $d/\Lambda = 0.8$, and Fig. 3(a) and Fig. 4(b) for $d/\Lambda = 0.4$), we note that the same approximation function can be applied for both wavelengths ($\lambda = 1.55$ and 1.0 μm) although the actual MFD is different. That is, the field is concentrated more in the silica with less field intensity entering the air holes when $\lambda = 1.0$ μm.

$$w = \frac{2\int\int_{-\infty}^{\infty}\phi(x,y)\mathrm{sech}\left(\frac{x}{w}\right)\mathrm{sech}\left(\frac{y}{w}\right)\left\{x\tanh\left(\frac{x}{w}\right) + y\tanh\left(\frac{y}{w}\right)\right\}dxdy}{\int\int_{-\infty}^{\infty}\phi(x,y)\mathrm{sech}\left(\frac{x}{w}\right)\mathrm{sech}\left(\frac{y}{w}\right)dxdy} \tag{6}$$

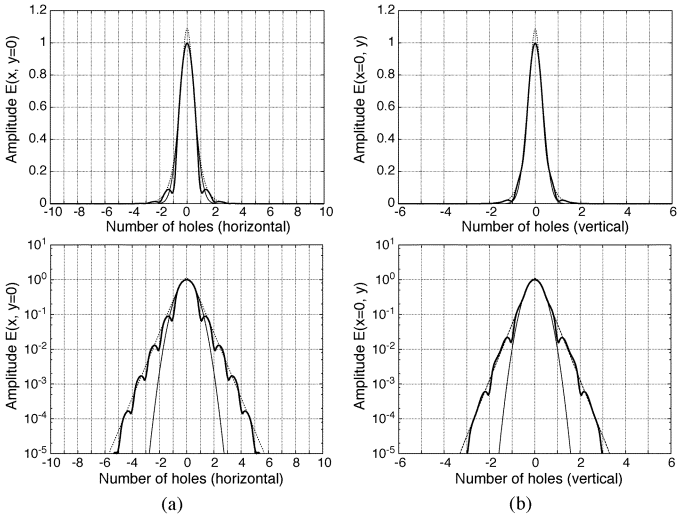

Fig. 3. Comparison of the actual PCF field distribution (thick solid curve) with the fitted Gaussian (thin solid curve) and sech (dotted curve) profile for $d/\Lambda = 0.4$. Linear (above) and log (below) scales. The mode is plotted along (a) x and (b) y axis.

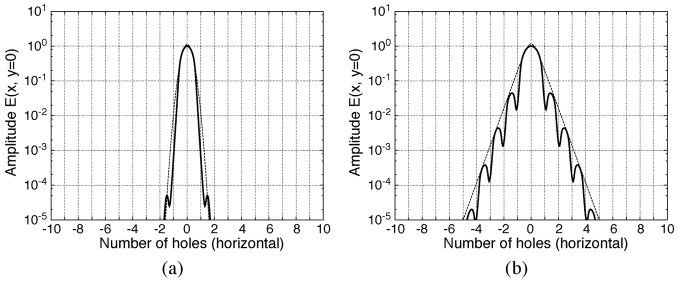

Fig. 4. Acutual PCF distribution for $\lambda = 1.0\ \mu$m when (a) $d/\Lambda = 0.8$ and (b) 0.4 (solid curves), compared with the fitted Gaussian and sech profile, respectively (dotted curves). The mode is plotted along x axis.

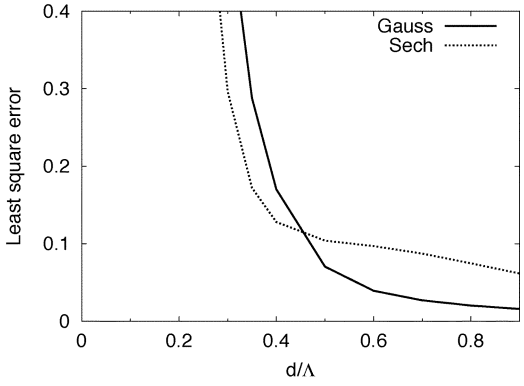

Fig. 5. Least square error in the Gaussian and sech approximations ($\lambda = 1.55\ \mu$m).

Fig. 5 summarizes the relationship between d/Λ values and the least square error $I(w)$ occured in Gaussian and sech approximations, which are evaluated from (2) and (5) when $\lambda = 1.55\ \mu$m. When $d/\Lambda > 0.45$, a Gaussian profile gives a better approximation of the mode field, whereas, for $d/\Lambda < 0.45$, sech yields a better approximation. It is interesting to note that the regime where the mode field is better fitted to a sech function overlaps with the endlessly single-mode operation regime $d/\Lambda > 0.43$ [13]. This implies that a mode field in the endlessly single-mode regime cannot be described by a Gaussian function and, hence, the analogy with SIFs is not applicable in this regime. The large error seen in $d/\Lambda < 0.3$ is due to weak field confinement, where there are many mode field dips that are not taken into account in the present approximation.

IV. Conclusion

We proposed least square Gaussian and sech approximations for the fundamental mode field profile in PCF. The mode field distribution in PCF depends strongly on the the air hole structure in the cladding. For large values of d/Λ, i.e., strongly guiding structures, the mode field is fitted well by a Gaussian. In this regime, the properties of PCF can be described by analogy with the equivalent SIF, whose refractive index in the cladding is given by the effective index of the cladding mode. However, for small d/Λ values, i.e., weakly guiding structures, a sech function describes the mode field more accurately, especially in the tail of the field. This implies that the analogy with SIF is no longer valid in this region. The approximation described here allows us to obtain the overlap integral analytically resulting in the easy evaluation of the coupling efficiency, splice loss, and reflection.

References

[1] J. C. Knight, T. A. Birks, P. St. J. Russel, and D. M. Atkin, "All-silica single-mode optical fiber with photonic crystal cladding," *Opt. Lett.*, vol. 21, no. 19, pp. 1547–1549, Oct. 1996.

[2] T. A. Birks, J. C. Knight, and P. St. J. Russel, "Endlessly single-mode photonic crystal fiber," *Opt. Lett.*, vol. 22, no. 13, pp. 961–963, July 1997.

[3] W. H. Reeves, J. C. Knight, P. St. J. Russel, and P. J. Roberts, "Demonstration of ultra-flattened dispersion in photonic crystal fibers," *Opt. Exp.*, vol. 10, no. 14, pp. 609–613, July 2002.

[4] J. C. Knight, J. Arriaga, T. A. Birks, A. Ortigosa-Blanch, W. J. Wadsworth, and P. St. J. Russel, "Anomalous dispersion in photonic crystal fiber," *IEEE Photon. Technol. Lett.*, vol. 12, no. 7, pp. 807–809, July 2000.

[5] J. C. Knight, T. A. Birks, R. F. Cregan, P. St. J. Russel, and J.-P. de Sandro, "Large mode area photonic crystal fiber," *Electron. Lett.*, vol. 34, no. 13, pp. 1347–1348, June 1998.

[6] N. G. R. Broderick, T. M. Monro, P. J. Bennett, and D. J. Richardson, "Nonlinearity in holey optical fibers: Measurement and future opportunities," *Opt. Lett.*, vol. 24, no. 20, pp. 1395–1397, Oct. 1999.

[7] D. Marcuse, "Loss analysis of single-mode fiber splices," *Bell Syst. Tech. J.*, vol. 56, no. 5, pp. 703–718, May 1977.

[8] M. Koshiba and K. Saitoh, "Structural dependence of effective area and mode field diameter for holey fibers," *Opt. Exp.*, vol. 11, no. 15, pp. 1746–1756, July 2003.

[9] B. T. Kuhlmey, R. C. McPhedran, C. M. de Sterke, P. A. Robinson, G. Renversez, and D. Maystre, "Microstructured optical fibers: Where's the edge?," *Opt. Exp.*, vol. 10, no. 22, pp. 1285–1290, Nov. 2002.

[10] N. A. Mortensen, J. R. Folkenberg, M. D. Nielsen, and K. P. Hansen, "Modal cutoff and the V parameter in photonic crystal fibers," *Opt. Lett.*, vol. 28, no. 20, pp. 1879–1881, Oct. 2003.

[11] J. R. Folkenberg, N. A. Mortensen, K. P. Hansen, T. P. Hansen, H. R. Simonsen, and C. Jakobsen, "Experimental investigation of cutoff phenomena in nonlinear photonic crystal fibers," *Opt. Lett.*, vol. 28, no. 20, pp. 1882–1884, Oct. 2003.

[12] R. Scarmozzino, A. Gopinath, R. Pregla, and S. Helfert, "Numerical techniques for modeling guided-wave photonic devices," *IEEE J. Select. Topics Quantum Electron.*, vol. 6, pp. 150–162, Jan. 2000.

[13] M. Koshiba, "Full-vector analysis of photonic crystal fibers using the finite element method," *IEICE Trans. Electron.*, vol. E85–C4, pp. 881–888, Apr. 2002.